Progress In Electromagnetics Research C, Vol. 117, 145–157, 2021

Dual-Band Waveguide Fed Hollow Cylindrical Dielectric Resonator Antenna

Varghese Sheeba[1, *], Parambil Abdulla[1], Baby A. Mary[2], Puthenveetil M. Jasmine[3], and Kunnath K. Ansha[1]

Abstract—In this paper, we present a waveguide-fed hollow cylindrical dielectric resonator antenna (CDRA) with dual-band operation and its modified structure for wider bandwidth and enhanced gain operation. The distinctive nature of the structure provides two bands having resonant frequencies at 8.46 GHz and 9.24 GHz with maximum gains of 5.37 dBi and 6.86 dBi respectively with a single dielectric resonator antenna (DRA). The dual-band is achieved due to the resonance of DRA and the air column inside it. Excellent coupling is achieved in both bands. The dual-band structure is modified by changing the volume of the air column inside the CDRA keeping all other parameters constant to result in a wider band and high gain antenna. A bandwidth of 7.9% with a resonant frequency of 9.0 GHz and a maximum gain of 8.14 dBi is obtained for the modified structure.

1. INTRODUCTION

The dynamic advancements in modern wireless communication demand high-frequency operation. As the antenna is a crucial component in the communication systems, it is vital to design it optimally for the fulfillment of the required characteristics. As the operating frequency goes high, conventional metallic antennas suffer from conduction loss due to the finite conductivity of the metal, and in turn, efficiency decreases [1]. Dielectric resonator antenna can be used as a better alternative to microstrip antennas and metallic antennas at higher frequencies, owing to the absence of conductor loss and surface waves [2]. Besides this, DRA offers high Q, small size, very low dielectric loss, flexibility in shape, and high radiation efficiency [3]. All these characteristics of the DRA make it a favorable candidate for high-frequency communication. DRA can be excited with different feeding lines like microstrip [4], coplanar waveguide (CPW) [5], co-ax feed [6], conformal strip [7], and metallic waveguide [8]. Among these, the waveguide feed is one of the best feeding techniques, as it provides excellent shielding between the inner and outer regions with negligible radiation loss [9], and in turn, DRA and waveguide form a brilliant pair for high-frequency communication systems. But when low permittivity DRAs are excited by direct waveguide feed, famished coupling is resulted [10].

Dual-band operation of DRAs with different feeding techniques has been investigated in the literature [11–13]. But only a few works have been reported for the dual-band operation with waveguide feed. Leung and So describe a dual-band waveguide fed cylindrical DRA with resonant frequencies 4.33 GHz and 4.7 GHz, which consists of a second dielectric resonator (DR) that is placed below the slot in the waveguide [14]. This results in a second band and enhanced coupling, but the structure has the limitations of fabrication difficulty and low gain and it requires two DRAs to achieve dual-band. Another dual-band operation of waveguide fed three-layer hemispherical DRA (HDRA) is realized in [15] that employs multiple DRAs for attaining dual-band and coupling enhancement. In

Received 30 October 2021, Accepted 22 December 2021, Scheduled 30 December 2021

* Corresponding author: Sheeba Varghese (sheebavarghese.cusat@gmail.com).

[1] Division of Electronics, Cochin University of Science and Technology, Cochin 682022, Kerala, India. [2] SECTE, University of Wollongong, Wollongong, NSW 2522, Australia. [3] Department of Electronics, MES College, Marampally, Kerala, India.

this structure, the number of DRAs increases the cost as well as the fabrication difficulty. Different coupling enhancement techniques for waveguide-fed DRAs are achieved by a stair-shaped waveguide [16], tapered waveguide [17], and capacitive waveguide junction [8]. All these structures are of single-band operation and suffer from fabrication intricacy. Different feeding techniques such as coaxial probe [18], substrate integrated waveguide (SIW) [19, 20], and microstrip feed [21] are reported in the literature for dual-band and wideband operations. In [18–20], more than one DRA element is used to get dual-band and wide bandwidth. In [20], four different DRA elements are employed to get wider bandwidth. This increases the cost of the overall system. In [21], a DRA in the shape of an inverted umbrella is used to achieve a bandwidth of 28%, but the realization of the DRA structure is complex, and the gain is also low.

In this paper, we propose a simple and efficient coupling technique, in which a single hollow cylindrical DRA achieves the dual-band operation with fairly good gain. In the proposed structure, without using any additional component very good matching is achieved by simply introducing a cross-slot (a combination of horizontal and vertical slots) on the ground plane at the shorted end of the waveguide. By slightly changing the air column inside the DRA, a wideband operation is observed with an increase in gain. The proposed antenna is very easy to fabricate and does not require any additional components for achieving these two objectives. The structure is simulated using Ansoft HFSS, and parametric analysis has been conducted to optimize the different parameters involved in the design. The measurement has been carried out using R&S ZVL 13 network analyzer, and the simulated results were analyzed and verified experimentally.

2. ANTENNA CONFIGURATION AND DESIGN

The proposed antenna configuration consists of a hollow cylindrical DRA, ground plane, with two slots that are cut in a cross shape, and WR-90 waveguide. The ground plane of dimension $gd \times gd \times t$ is placed on one of the ends of the waveguide of cross-section $a \times b$ and length l. Two rectangular slots of dimensions $sl \times sw \times t$ and $sa \times sb \times t$ are cut on the ground plane to excite the DRA, and these rectangular slots together make a cross-shaped slot. The horizontal and vertical slots are off-centered by u and v respectively in $+x$ direction. The hollow cylindrical DRA made of Al_2O_3 — ceramic (alumina) of permittivity ε_r, outer radius d_r, inner radius a_r, outer height h, and inner height h_1 is placed with its open end on the ground plane. The cross-sectional view, top view, and 3D structure of the antenna configuration are shown in Figures 1(a), (b), and (c), respectively.

The proposed antenna is designed to resonate in two bands in the X-band frequency range with resonant frequencies 8.48 GHz and 9.2 GHz. A hollow cylindrical DRA of outer radius 10 mm and outer height of 6 mm is taken as the resonating element. An air column of radius 6.5 mm and height 3 mm is introduced in the DRA centrally. The air column inside the DRA substantially affects the effective permittivity and Q-factor which in turn, reduces the permittivity [22] to 4.8 approximately from 9.8. The dual-band operation is achieved since CDRA, air column, and slots resonate as partially independent mechanisms. DRA resonant frequency depends on the mode of operation, geometrical dimensions, and effective relative permittivity [23]. In the designed structure, the DRA is made to operate at $HEM_{12\delta-}$ like and $HEM_{12\delta}$ mode in first and second bands. The first resonance band is obtained as the result of resonance of DRA, air column, and slot. The DRA is excited at $HEM_{12\delta-}$ like mode, and the dimensions of the slot and air column determine the first resonant frequency. The resonant frequency of the cylindrical DRA excited at $HEM_{12\delta}$ mode is given by the equation

$$f_{r(\mathrm{GHz})} = \frac{30(k_0 a)}{2\pi a_{\mathrm{cm}}} \tag{1}$$

where a_{cm} is the radius of the DRA; ε_{reff} is the effective permittivity; $k_o a$ is the wavenumber which can be determined by equation

$$k_0 a = \frac{\left\{3.72 + 0.4464x + 0.2232x^2 + 0.0521x^3 - 2.65e^{-1.25x(1+4.7x)}\right\}}{\sqrt{\varepsilon}_{reff.}} \tag{2}$$

where $x = \frac{a}{2h}$, from which the resonant frequency is obtained as 9.2 GHz [24].

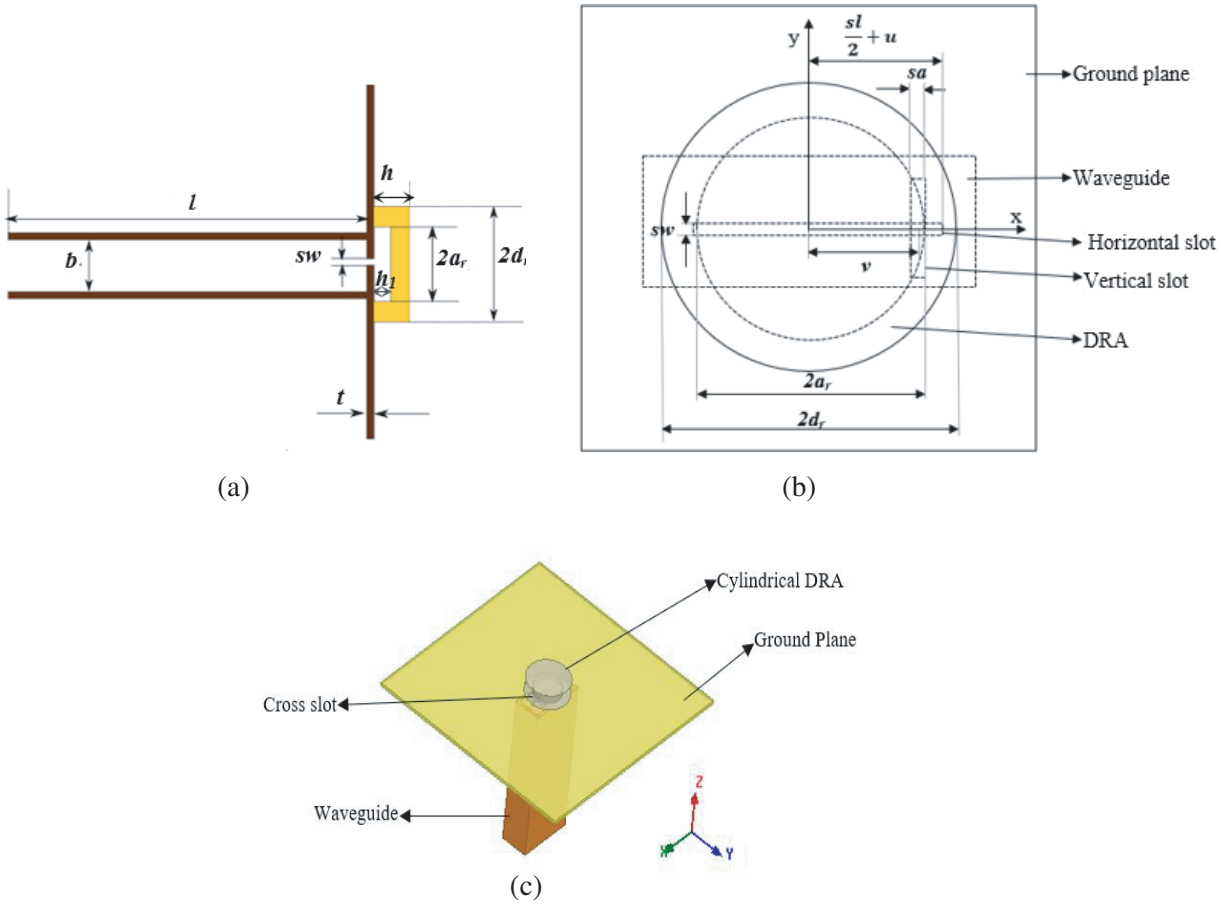

Figure 1. Antenna configuration. (a) Cross-sectional view. (b) Top-view. (c) 3D structure.

In waveguide-fed DRAs, the direct coupling of the DRA to the waveguide introduces inductive susceptance, and effective coupling is not possible [10]. To overcome this drawback, the inductive susceptance must be nullified by its counterpart. This is achieved by the air column inside the DRA and the cross-slot placed at the shorted end of the waveguide, and it results in impedance matching as well as efficient coupling. The different parameters involved in the design are analyzed and optimized to give an excellent result. The optimized values of various parameters are tabulated in Table 1.

Table 1. Optimized parameters of the proposed antenna.

Parameter	Value	Parameter	Value
a	22.86 mm	sb	9.0 mm
b	10.16 mm	u	1.8 mm
l	60.00 mm	v	6.5 mm
gd	100.0 mm	d_r	10 mm
t	1.30 mm	a_r	6.5 mm
sl	15.8 mm	h	6.0 mm
sw	1.00 mm	h_1	3.0 mm
sa	1.50 mm	ε_r	9.8

3. PARAMETRIC ANALYSIS

The antenna performance depends on various parameters such as slot dimensions, offsets of the slots, inner and outer heights, and inner and outer radii of the DRA. The effect of these parameters has been studied by performing the parametric analysis using Ansoft HFSS.

3.1. Length sl and Width sw of the Horizontal Slot

Figures 2(a) and (b) depict the variation of $|S_{11}|$ as the function of the length *sl* and width *sw* of the horizontal slot, respectively. As the slot length is changed from 15.0 mm to 15.8 mm in 0.4 mm steps, keeping all other parameters constant it is observed that the resonant frequency of the first band is decreased from 8.5 GHz to 8.39 GHz, but the change in the second band is negligible. The change in the width of the horizontal slot has an appreciable influence on the coupling and the resonant frequencies. When the width of the horizontal slot is changed from 0.8 mm to 1.2 mm with a step size of 0.2 mm, it can be seen that there is an upward shift in the two resonant frequencies, and the coupling is maximum when $sw = 1$ mm.

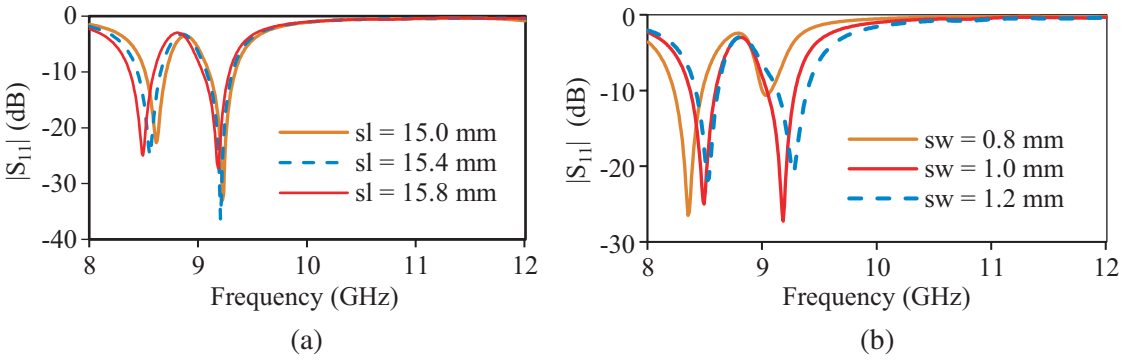

Figure 2. $|S_{11}|$ as the function of (a) length of the horizontal slot, (b) width of the horizontal slot.

3.2. Length sa and Width sb of the Vertical Slot

Figures 3(a) and (b) show the variation of the $|S_{11}|$ parameter with respect to the change in length *sa* and width *sb* of the vertical slot. From this it is clear that the variation of length *sa* of the vertical slot affects the coupling only, but not the resonant frequencies. The width of the slot *sb* is also a determining factor of coupling of the second band. As it is varied from 8.8 mm to 9.2 mm in a step size of 0.2 mm,

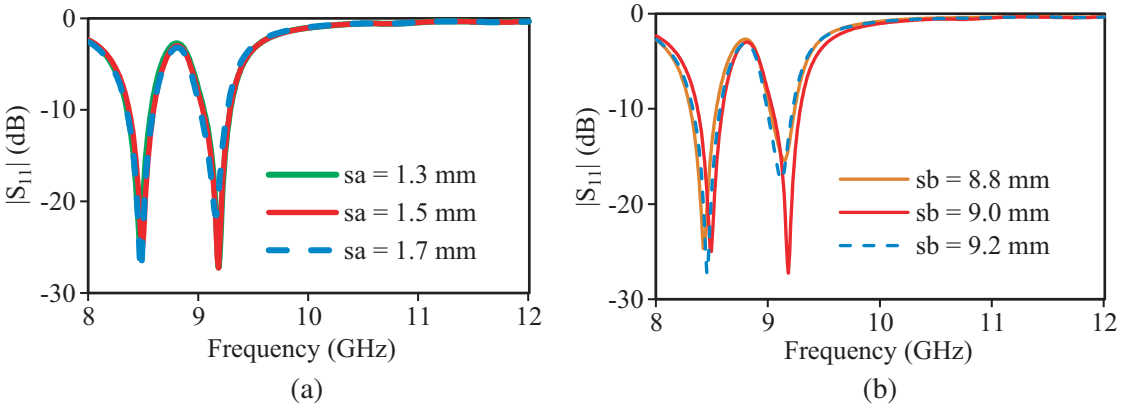

Figure 3. $|S_{11}|$ as a function of (a) length of the vertical slot, (b) width of the vertical slot.

keeping all other parameters constant, negligible change in the resonant frequency is observed. But excellent coupling is obtained at $sa = 1.5\,\text{mm}$ and $sb = 9\,\text{mm}$.

3.3. Offset u of the Horizontal and v of the Vertical Slots

The offset positions of the two slots on the ground plane are significant parameters that determine the return loss characteristics of the proposed antenna. A parametric study has also been done on the offset u of the horizontal slot and v of the vertical slot in $+x$ direction which are plotted in Figures 4(a) and (b), respectively. Figure 4(a) reveals that the best-approximated value of u is 1.8 mm. As the offset v of the vertical slot is varied from 6.3 mm to 6.7 mm in equal steps, it is observed that both the resonant frequencies shift to the left, and also the coupling is affected. From the parametric analysis, the value of v is optimized to 6.5 mm.

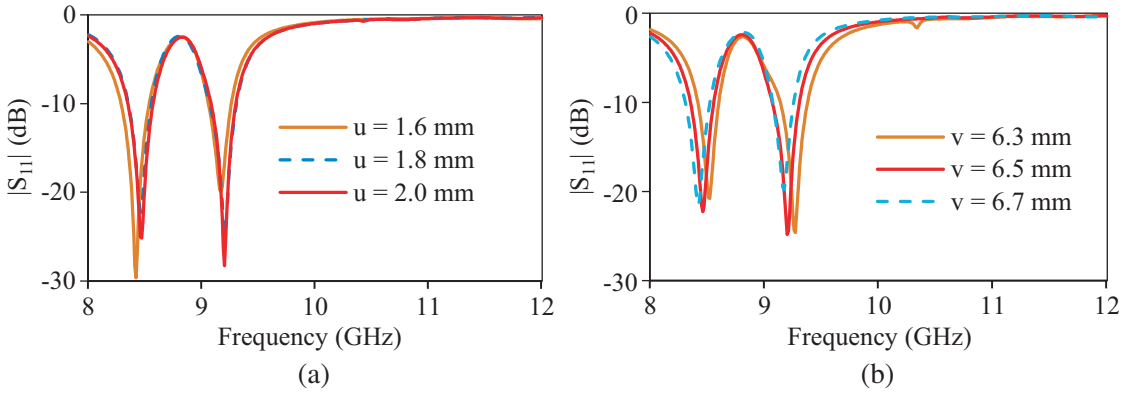

Figure 4. $|S_{11}|$ as a function of (a) offset of the horizontal slot, (b) offset of the vertical slot.

3.4. Radius d_r and Height h of the DRA

Figure 5(a) shows the variation of the $|S_{11}|$ of the proposed antenna with the variation of the radius d_r of the DRA. It is observed that it has a significant effect on both resonant frequencies and coupling. The best result is obtained at $d_r = 10\,\text{mm}$. The height of the DRA is a design factor of the resonant frequencies and coupling of the antenna. As it varies from 5.8 mm to 6.2 mm, both the resonant frequencies and the coupling are found to be increased as shown in Figure 5(b).

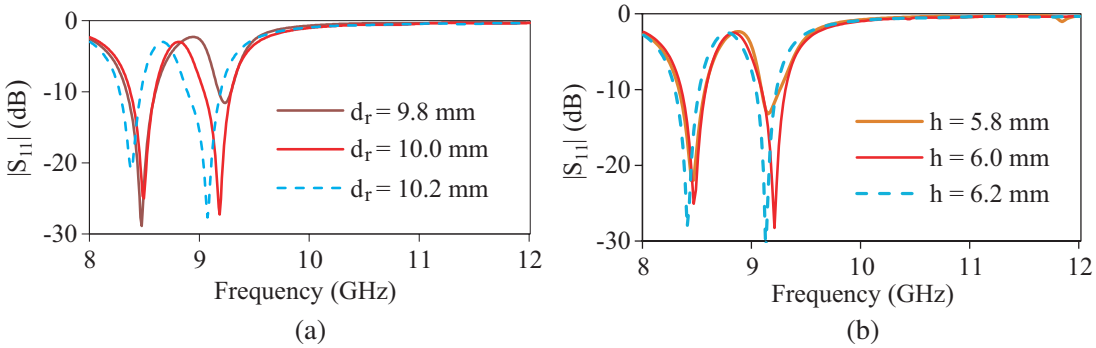

Figure 5. $|S_{11}|$ as a function of (a) radius of the DRA, (b) height of the DRA.

4. RESULTS AND DISCUSSIONS

Simulations of the proposed structure with optimized parameters have been carried out using Ansoft HFSS to analyze the antenna performance. The prototype of the structure has been fabricated, and the side-view and inner side of the hollow DRA are shown in Figures 6(a) and (b), respectively. The measurements were taken using R&S ZVL13 network analyzer in an open environment. Reflection coefficient, radiation patterns, gain, and field distributions are studied and analyzed.

(a) (b)

Figure 6. (a) Side view of prototype. (b) Inner side of hollow CDRA.

4.1. Reflection Coefficient

The $|S_{11}|$ parameter of an antenna determines its coupling efficiency. At resonant frequencies, maximum power is coupled to the DRA, and it makes the DRA radiate to the atmosphere. Figure 7 compares the measured and simulated reflection coefficients of the designed antenna. The simulated result exhibits a dual-band operation with resonant frequencies 8.48 GHz and 9.20 GHz. The lower frequency of the first band is 8.35 GHz and is extended up to 8.60 GHz giving an impedance bandwidth of 2.9%. The second band has an impedance bandwidth of 3.05% with a band ranging from 9.03 GHz to 9.31 GHz.

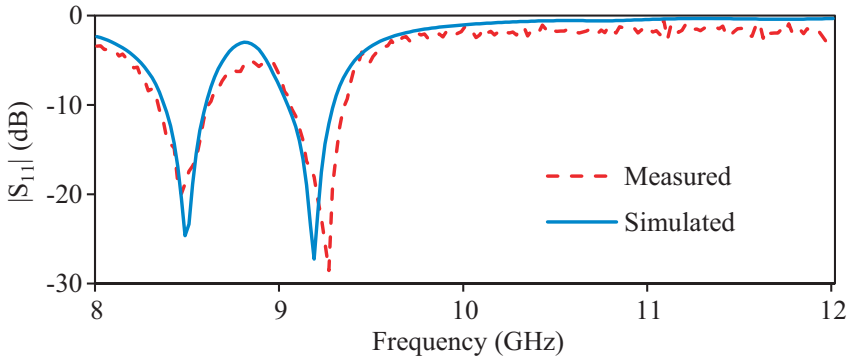

Figure 7. Measured and simulated $|S_{11}|$.

The measured reflection coefficient exhibits an excellent agreement with the simulated results, as it provides the first resonant band from 8.33 GHz to 8.61 GHz with a resonant frequency of 8.46 GHz and 10 dB bandwidth of 3.3%. The second band is from 9.05 GHz to 9.35 GHz with a resonant frequency of 9.24 GHz. The 10 dB impedance impedance bandwidth is obtained as 3.26%. 20 MHz of downward shift and 40 MHz of upward shift on first and second resonant frequencies respectively are shown by the

antenna during the measurements. These slight variations in resonant frequencies may be due to the error in fabrication and the air gap present between the DRA and ground plane [16].

4.2. Radiation Patterns

The radiation pattern of an antenna is very significant as the directivity, gain, and polarization can be inferred from this. Figures 8(a) and (b) show the radiation patterns of the proposed antenna in E-plane and H-plane at 8.48 GHz, and Figures 8(c) and (d) give the E-plane and H-plane radiation patterns at 9.2 GHz. Figures 9(a) and (b) depict the 3D radiation patterns at 8.48 and 9.20 GHz, respectively. From the simulated and measured radiation patterns, it is obvious that the antenna is linearly polarized, and the co-polarization differs from cross-polarization by more than 25 dB in the broadside at both frequencies. The variation in the measured and simulated cross-polarizations is the effect of noise as the measurement is taken in the open environment.

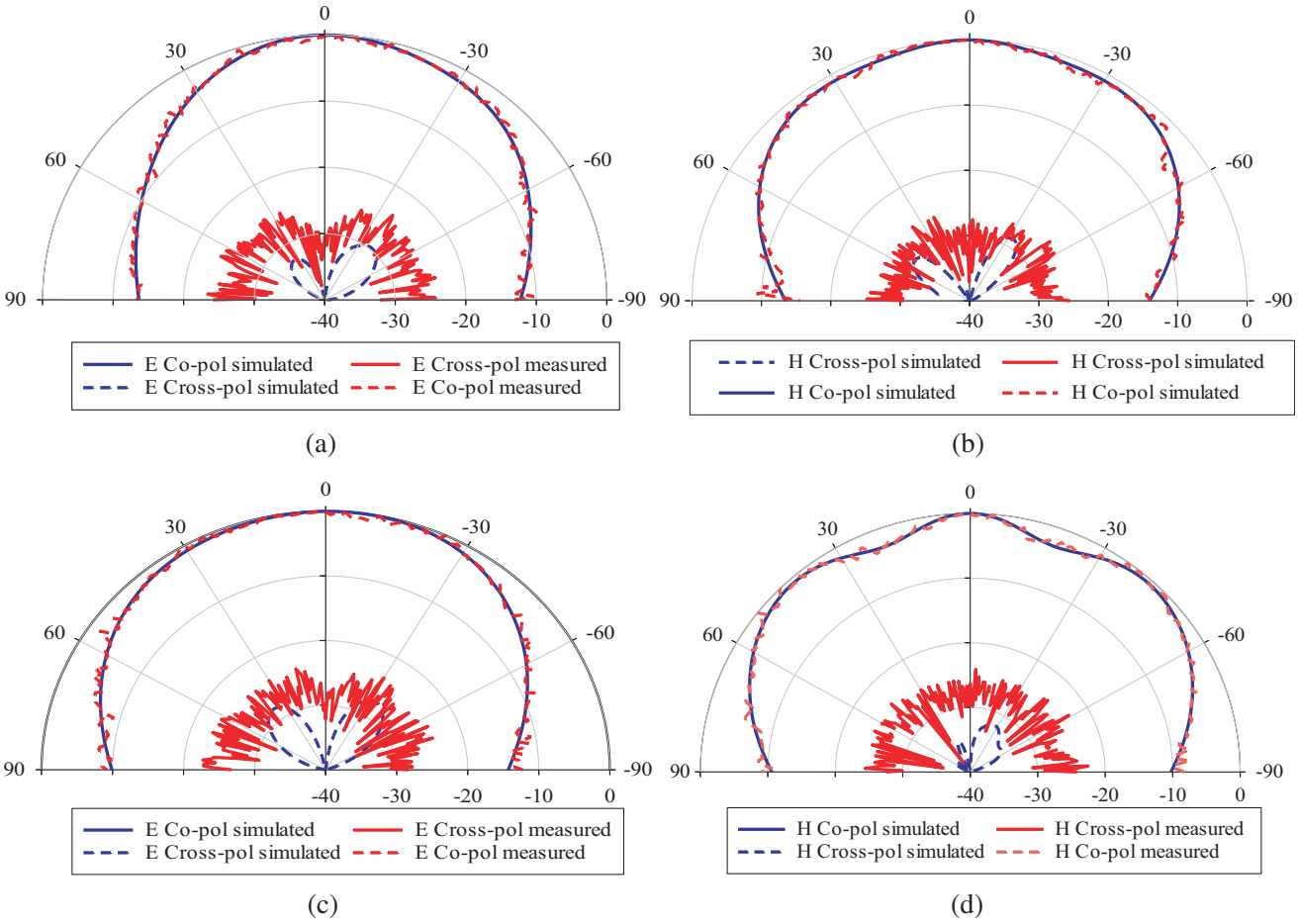

Figure 8. (a) E-plane radiation pattern at 8.48 GHz. (b) H-plane radiation pattern at 8.48 GHz. (c) E-plane radiation pattern at 9.2 GHz. (d) H-plane radiation pattern at 9.2 GHz.

4.3. Gain

The gain is a vital parameter of an antenna, and it indicates the ability of the antenna to convert the input power to radio waves. Figure 10 depicts the simulated and measured gains for the resonant bands 8.33 GHz to 8.61 GHz and 9.05 GHz to 9.35 GHz. It illustrates that the measured gain adheres to the simulated gain in both bands. The measured maximum gain of 5.37 dBi is obtained at 8.45 GHz in the first band. In the second band, the measured maximum gain is 6.86 dBi at 9.15 GHz.

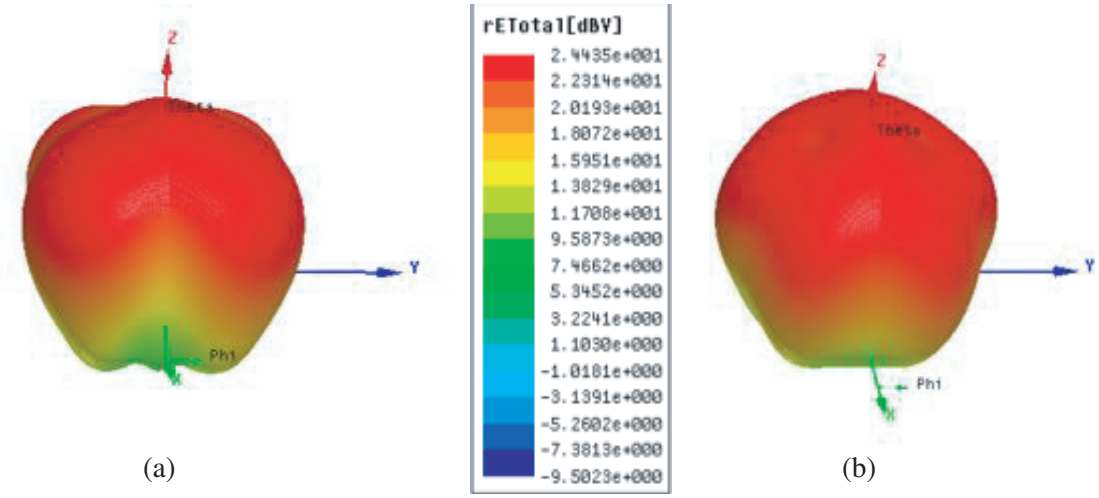

Figure 9. 3D radiation plot for dual-band operation at (a) 8.48 GHz, (b) 9.2 GHz.

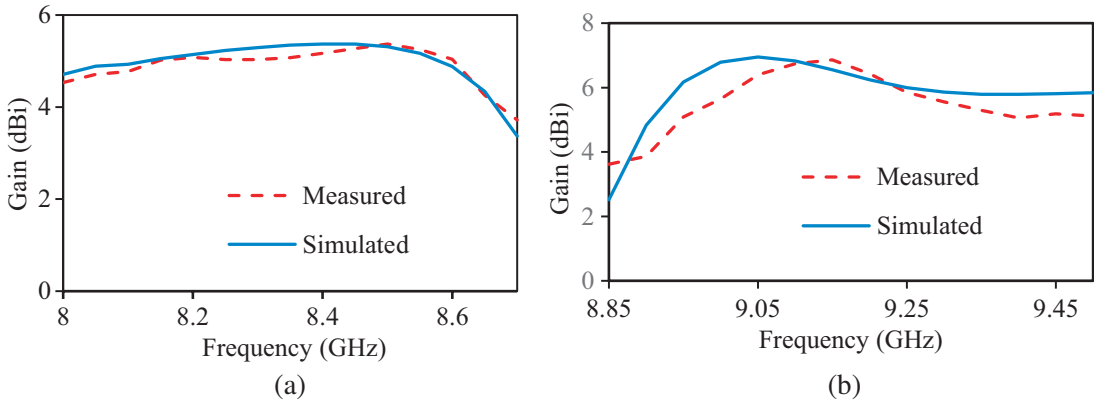

Figure 10. Measured and simulated gain of (a) band 8.33–8.61 GHz, (b) band 9.05–9.35 GHz.

4.4. Field Distribution

An external field distribution is associated with each mode of DRA operation. By exciting different modes in DRA different field patterns can be obtained. The proposed DRA is excited in two higher-order modes viz $HEM_{12\delta-}$ like mode at 8.48 GHz and $HEM_{12\delta}$ mode at 9.2 GHz. The E-filed distributions in xy-plane at the first band and second band are shown in Figures 11(a) and (b), respectively.

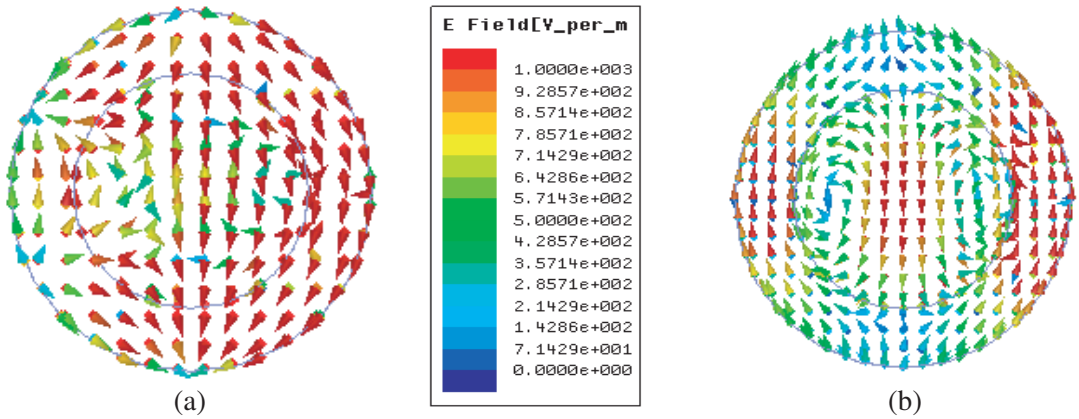

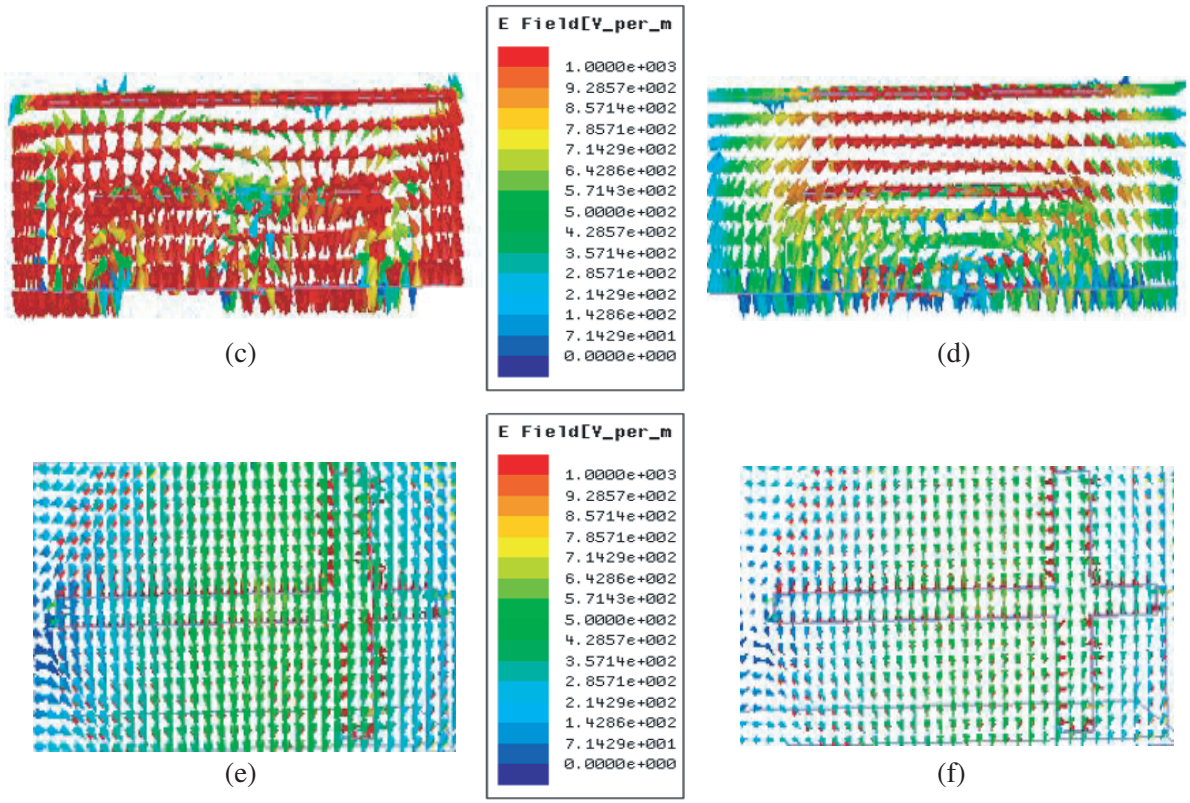

Figure 11. E-field distribution of the DRA in xy plane at (a) 8.48 GHz, (b) 9.2 GHz, E-field distribution of DRA in xz plane at (c) 8.48 GHz, (d) 9.2 GHz and E-field distribution in the slots in xy plane at (e) 8.48 GHz, (f) 9.2 GHz.

Figures 11(c) and (d) depict the E-filed distributions in xy-plane at 8.48 and 9.2 GHz. Figures 11(e) and (f) describe the field distributions in the slots at the resonant frequencies. It is observed that E-field is maximum at the slot edges, and hence due to the field discontinuity, the power will be radiated through the slot and coupled to the DRA.

5. WIDEBAND OPERATION

The structure is modified to make the two resonant bands overlap each other and hence increase the bandwidth and gain of the antenna. The CDRA and the volume of the air column inside the DRA

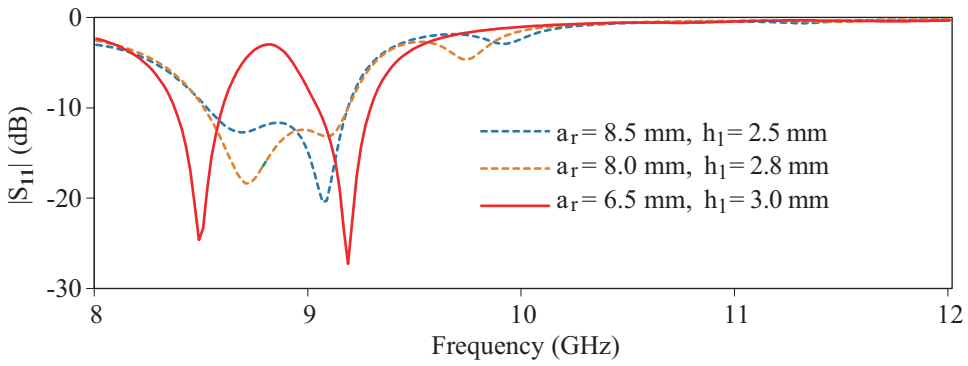

Figure 12. Variation of $|S_{11}|$ with the variation of the radius and height of the air column.

determine the resonant frequencies and bandwidth. As the volume of the air column is changed, without changing any other parameters, the wider band operation with increased bandwidth and enhanced gain has resulted. The parametric study on the variation of the air column inside the DRA is shown in Figure 12. The wider band is because as the volume of the air column changes, the effective permittivity and Q-factor of the DRA change. As a result, the first resonant band is shifted upwards and overlaps with the second resonant band forming a single band with increased bandwidth. When the inner radius of the CDRA is increased from 6.5 mm to 8.5 mm and inner height decreased from 3 mm to 2.5 mm keeping all other parameters constant, the single band operation with enhanced bandwidth and high gain is achieved. Simulations have been conducted using Ansoft HFSS, and measurements of the prototype are taken using R&S ZVL13 network analyzer.

5.1. Simulated and Measured Results

The simulated and measured results of various parameters of the antenna are in good agreement with each other. The simulated results show that the antenna resonates at 9.06 GHz with a bandwidth of 7.6% and a maximum gain of 8.12 dBi.

The measured results give a bandwidth of 7.9% with a resonant frequency of 9.0 GHz and a maximum gain of 8.14 dBi. The bandwidth is increased, and the gain is also enhanced. A tolerable downward shift of 60 MHz in the resonant frequency and 110 MHz of an upward shift in the resonance band are observed during measurement. This variation in the measured result is due to the air gap present between the ground plane and DRA [16]. Figures 13(a) and (b) show $|S_{11}|$ and the gain of the single band structure. Radiation patterns in E-plane and H-plane are also plotted and depicted in Figures 14(a) and (b), respectively. Figure 14(c) describes the 3D radiations of the proposed antenna for single-band operation. The patterns show that the co-polarization differs by a minimum of 30 dB from the cross-polarization.

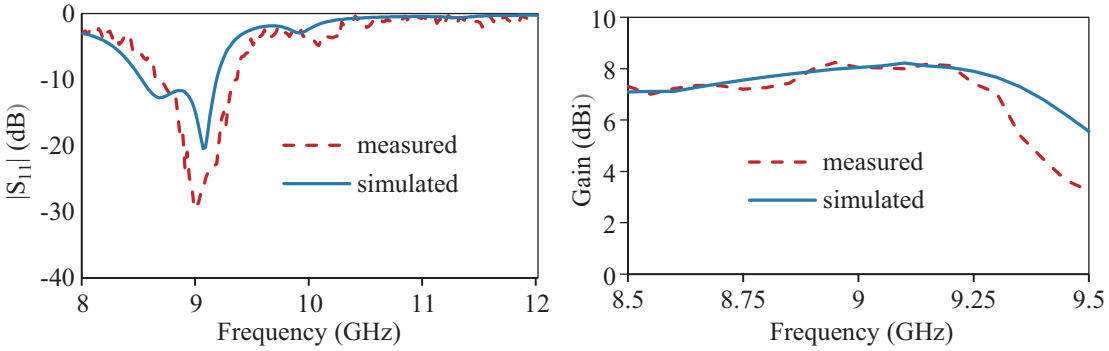

Figure 13. (a) Measured and simulated $|S_{11}|$. (b) Measured and simulated gain.

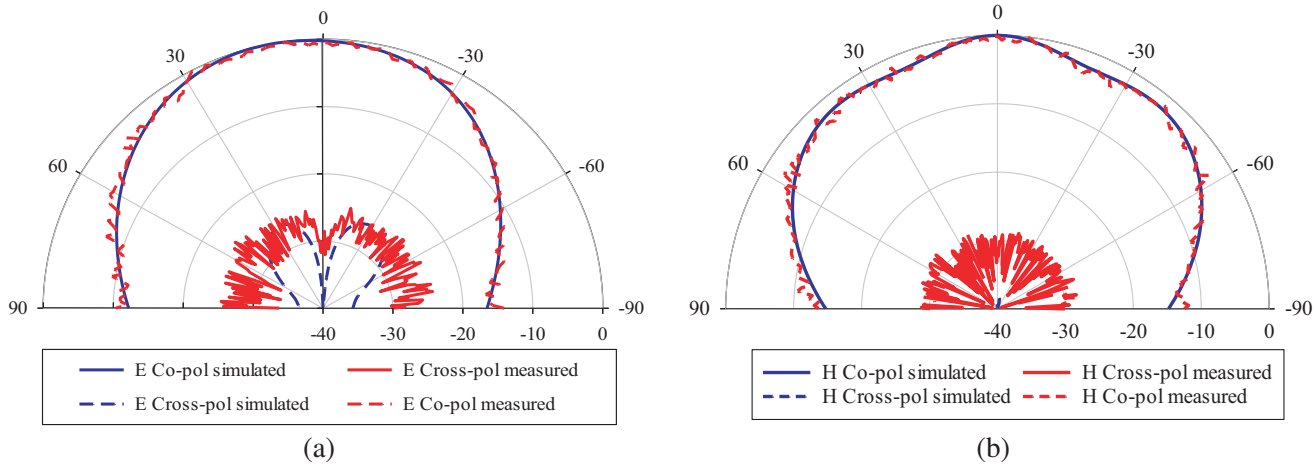

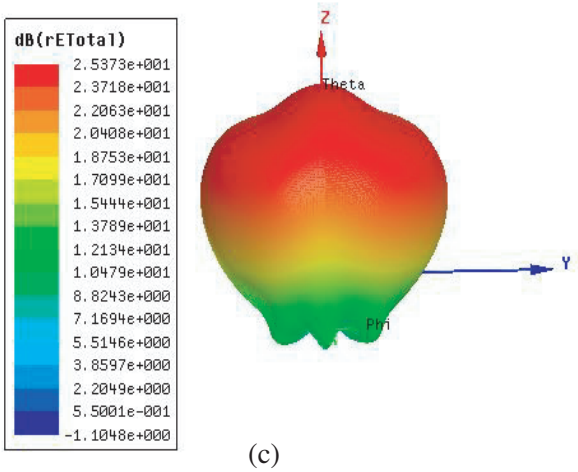

(c)

Figure 14. (a) E-plane radiation pattern. (b) H-plane radiation pattern. (c) 3D radiation plot for single-band operation.

Table 2. Comparison of the proposed antennas with other similar works.

Reference	**Shape of DRA***	**Feeding Technique**	**No. of DRAs**	**No. of bands**	**Size of DRA** (mm)**	ε_r	**f_r** (GHz)	**BW %**	**Max. Gain (dBi)**
[8]	RDRA	waveguide	1	1	$l = 20.4$ $b = 6.21$ $h = 6.21$	10	8.90	3.48	not mentioned
[14]	CDRA	waveguide	2	2	$r = 6.0, 6.0$ $h = 10.1, 10.1$	16 16	4.33 4.70	4.36 3.17	4.4 4.4
[15]	HDRA	waveguide	3	2	$r = 13.5,$ $16.2, 23.9$	1 4.3 9.5	8.82 10.46	not mentioned	6.1 6.4
[16]	HDRA	waveguide	1	1	$r = 7.5$	9.8	9.2	7.4	5.7
[17]	HDRA	waveguide	1	1	$r = 6.27$	9.8	10.78	4.5	5.5
[18]	L-shaped (MIMO)	co-axial	2	2	$l = 20, 10$ $b = 20, 10$ $h = 5, 2$	10 30	3.6 5.2	9.97 8.88	5.7 6.61
[19]	RDRA	SIW	2	2	$l = 10, 10$ $b = 7, 7$ $h = 3.81, 3.81$	10.2 10.2	8.58 10.62	6.76 6.76	6.0 6.24
[20]	RDRA (MIMO)	SIW	4	2	$l = 15.84$ $b = 5$ $h = 0.254$	9.8	27.4 36.58	24 12	9.1 9.9
[21]	Inverted umbrella	microstrip	1	1	$r = 20$ $h = 5$	10.2	6.25	28	5.2
Proposed structure 1	**HCDRA**	**waveguide**	**1**	**2**	$r = 10$ $h = 6.1$	**9.8**	**8.46** **9.24**	**3.3** **3.26**	**5.37** **6.86**
Proposed structure 2	**HCDRA**	**waveguide**	**1**	**1**	$r = 10$ $h = 6.1$	**9.8**	**9.0**	**7.9**	**8.14**

***** CDRA — cylindrical DRA, HDRA — hemispherical DRA, HCDRA — hollow cylindrical DRA.
****** r — radius, l — length, b — width, h — height.

6. COMPARISON WITH OTHER SIMILAR WORKS

The performance comparison of the proposed antenna with similar reported works in literature is tabulated in Table 2. Only a few investigations have been conducted in the dual-band operation of waveguide-fed DRA in literature. It can be seen that the proposed antenna exhibits good gain and dual-band operation with a single DRA. The comparable gain in other works has been obtained only with more than one DRA. Dual-band operation with fairly good gain and excellent coupling with a single DRA are the advantages of the proposed antenna. This can be easily converted to a wider band operation with high gain.

7. CONCLUSION

This work presents a simple coupling technique by introducing a cross-slot at the shorted end of the waveguide for the waveguide-fed DRA. The antenna configuration produces a dual-band operation. The two resonant frequencies are obtained at 8.46 GHz and 9.24 GHz with bandwidths of 3.3% and 3.26%, respectively. The structure shows maximum gains of 5.37 dBi and 6.86 dBi in the first and second bands with excellent coupling. The proposed antenna can be used in the field of maritime radio navigation applications and medical imaging. The dual-band antenna can be modified for wideband operation with enhanced gain by changing the air volume inside the CDRA resulting in the overlap of two bands. The modified structure resonates at 9.0 GHz with a bandwidth of 7.9% and a gain of 8.14 dBi.

REFERENCES

1. Cicchetti, R., A. Faraone, D. Caratelli, and M. Simeoni, "Wideband, multiband, tunable, and smart antenna systems for mobile and UWB wireless applications 2016," 2017.
2. Leung, K. W., E. H. Lim, and X. S. Fang, "Dielectric resonator antennas: From the basic to the aesthetic," *Proc. IEEE*, Vol. 100, No. 7, 2181–2193, 2012.
3. Keyrouz, S. and D. Caratelli, "Dielectric resonator antennas: Basic concepts, design guidelines, and recent developments at millimeter-wave frequencies," *Int. J. Antennas Propag.*, Vol. 2016, 2016.
4. Pan, Y. M. and S. Y. Zheng, "A low-profile stacked dielectric resonator antenna with high-gain and wide bandwidth," *IEEE Antennas Wirel. Propag. Lett.*, Vol. 15, 68–71, 2016.
5. Rao, Q., T. Denidni, A. Sebak, and and R. Johnston, "On improving impedance matching of a CPW fed low permittivity dielectric resonator antenna," *Progress In Electromagnetics Research*, Vol. 53, 21–29, 2005.
6. Leung, K. W., K. Y. A. Lai, K. M. Luk, and D. Lin, "Theory and experiment of a coaxial probe fed hemispherical dielectric resonator antenna," *IEEE Trans. Antennas Propag.*, Vol. 41, No. 10, 1390–1398, 1993.
7. Chu, L. C. Y., D. Guha, and Y. M. M. Antar, "Conformal strip-fed shaped cylindrical dielectric resonator: Improved design of a wideband wireless antenna," *IEEE Antennas Wirel. Propag. Lett.*, Vol. 8, 482–485, 2009.
8. Abdulla, P., Y. K. Singh, and A. Chakrabarty, "Coupling enhancement of waveguide-fed dielectric resonator antenna," *Microw. Opt. Technol. Lett.*, Vol. 53, No. 4, 769–770, Apr. 2011.
9. Eshrah, I. A., A. A. Kishk, A. B. Yakovlev, and A. W. Glisson, "Theory and implementation of dielectric resonator antenna excited by a waveguide slot," *IEEE Trans. Antennas Propag.*, Vol. 53, No. 1 II, 483–494, Jan. 2005.
10. Abdulla, P. and A. Chakrabarty, "Rectangular waveguide-FED hemispherical dielectric resonator antenna," *Progress In Electromagnetics Research*, Vol. 83, 225–244, 2008.
11. Chen, H. M., Y. K. Wang, Y. F. Lin, S. C. Lin, and S. C. Pan, "A compact dual-band dielectric resonator antenna using a parasitic slot," *IEEE Antennas Wirel. Propag. Lett.*, Vol. 8, 173–176, 2009.
12. Pan, Y. M., S. Y. Zheng, and B. J. Hu, "Design of dual-band omnidirectional cylindrical dielectric resonator antenna," *IEEE Antennas Wirel. Propag. Lett.*, Vol. 13, 710–713, 2014.

13. Gao, Y., B.-L. Ooi, and A. P. Popov, "Dual-band hybrid dielectric resonator antenna with CPW-fed slot," *Microw. Opt. Technol. Lett.*, Vol. 48, No. 1, 170–172, Jan. 2006.
14. Leung, K. W. and K. K. So, "Rectangular waveguide excitation of dielectric resonator antenna," *IEEE Trans. Antennas Propag.*, Vol. 51, No. 9, 2477–2481, Sep. 2003.
15. Kakade, A. B. and B. Ghosh, "Analysis of the rectangular waveguide slot coupled multilayer hemispherical dielectric resonator antenna," *IET Microwaves, Antennas Propag.*, Vol. 6, No. 3, 338–347, Feb. 2012.
16. Muhammed, J. P., A. Parambil, and R. P. Muhammad, "Analysis and experiment of stair-shaped waveguide-fed dielectric resonator antenna,"*IET Microwaves, Antennas Propag.*, Vol. 10, No. 4, 453–458, Mar. 2016.
17. Jasmine, P. M., P. Abdulla, and P. M. Raphika, "Rectangular waveguide fed DRA using tapered waveguide section," *Microw. Opt. Technol. Lett.*, Vol. 57, No. 9, 2025–2028, Sep. 2015.
18. Khan, A. A., M. H. Jamaluddin, S. Aqeel, J. Nasir, J. U. R. Kazim, and O. Owais, "Dual-band MIMO dielectric resonator antenna for WiMAX/WLAN applications," *IET Microwaves, Antennas Propag.*, Vol. 11, No. 1, 113–120, Jan. 2017.
19. Sharma, A., A. Sarkar, A. Biswas, and M. J. Akhtar, "Substrate integrated waveguide fed dual-frequency dual-linearly-polarized dielectric resonator antenna," *Int. J. Microw. Wirel. Technol.*, Vol. 10, No. 4, 505–511, May 2018.
20. Rajat Girjashankar, P. and T. Upadhyaya, "Substrate integrated waveguide fed dual band quad-elements rectangular dielectric resonator MIMO antenna for millimeter wave 5G wireless communication systems," *AEU — Int. J. Electron. Commun.*, Vol. 137, 153821, Jul. 2021.
21. Vinodha, E. and S. Raghavan, "A broadband inverted umbrella shaped cylindrical dielectric resonator antenna for 'WLAN' and 'C' band applications," *Int. J. RF Microw. Comput. Eng.*, Vol. 27, No. 6, e21100, Aug. 2017.
22. Petosa, A., *Dielectric Resonator Antenna Handbook*, Artech, 2007.
23. Petosa, A. and A. Ittipiboon, "Dielectric resonator antennas: A historical review and the current state of the art," *IEEE Antennas Propag. Mag.*, Vol. 52, No. 5, 91–116, Oct. 2010.
24. Luk, K. M. and K. W. Leung, *Dielectric Resonator Antennas*, Research Studies Press, 2003.